Comparison Between Predicted and Measured Chemiluminescence in an Unstable Rocket Combustor

M. J. Bedard[⋆] [†], *T. L. Fuller*[⋆], *S. V. Shardeshmukh*[⋆], *and W. E. Anderson*[⋆]
[⋆]*Purdue University*
610 Purdue Mall, West Lafayette, Indiana 47906, mbedard@purdue.edu
...
[†]Corresponding author

Abstract

Experimental measurements of the unsteady heat addition field, are critical. Chemiluminescence intensity is a function of pressure, strain rate, equivalence ratio, and turbulence level. These flame properties have large variations in unstable rocket combustion, thus chemiluminescence may not be a direct indicator of heat release. Detailed chemical kinetics modeling is used to investigate the relationship between chemiluminescence and heat release rate of the flame. The model is validated by comparing against recorded chemiluminescence. Comparison of the model with point measurements illustrates the relation between the heat release and the chemiluminecence during unstable combustion.

1. Introduction

Combustion instability is a common recurring problem for bi-propellant rocket engines. Decades of successful operation of rocket combustors has failed to yield a complete understanding of combustion instability.[1,2] Instabilities arise due to coupling between the natural acoustic modes of a combustor and the unsteady processes of combustion. High-frequency combustion instabilities in excess of 1000 Hz are detrimental to combustor performance and lead to catastrophic failures in engines due to over-pressure and overheating. Via acoustic coupling with hydrodynamics, combustor geometry is strongly correlated with the formation of instabilities, and, as a result, a complete characterization of this complex process may only be obtained during full scale engine testing. If the stability characteristics of the combustor can be adequately modeled, large savings can be made in the cost of engine development.

Currently available modeling techniques and technologies do not allow for complete simulation of a full scale combustor. Recently, however, high-fidelity CFD models have shown some ability of being able to match stability behavior in subscale experimental combustors with a limited domain ,[3–7,9] and historical rates in computational advancements suggest that computations including partial full scale geometry and multi-injector interactions will be possible in the next decade. An alternative strategy in the engine development cycle can take advantage of targeted full scale simulations with derived reduced order models from such high fidelity models accelerating the design process. This coalescence of experimentation and model validation should produce a complete and powerful model of combustion instability for rocket and other propulsion systems. The most complex part of this approach is the measurement and comparison of unsteady heat addition.

High fidelity CFD models of unstable combustion require a huge amount of computational resources. Modeling flow physics alone on length and time scales small enough to resolve critical flow mechanisms limits the capabilities of recent models. As a result, axisymmetric assumptions and simplified chemical kinetics models are typically used to represent very complex combustion systems. It has been suggested that three dimensional models with detailed chemical kinetics modeling are required to accurately capture the heat release process that is so critical to the development of an unstable combustion environment. [4,7]

The transfer of energy from the combustion of propellants to the acoustic energy field is the primary mechanism that creates acoustically coupled combustion instability. Testing of CFD models through experimentation is an integral step in the development of tools to predict and mitigate combustion instability in engine design. Predicted pressure modes alone can show excellent agreement to experimental data,[8,9] but

direct comparison of the combustion energy release is more challenging. A direct measurement of transient heat release in a practical combustor is not feasible and measurement techniques that do not interfere with the flame itself are limited. Collection of light emitted from chemiluminescent species in the flame is commonly employed to estimate locations of high heat release. This technique relies on several fundamental assumptions, such as the spatio-temporal coincidence of light emission and heat release, optical depth of the flame, and three-dimensional effects, all of which are addressed in the present study.

This study is a step towards quantitative comparison between the unsteady heat release measured in experiment and predicted by simulation and an investigation of the ability of chemiluminescence measurements to provide this comparison. To that end, two techniques are utilized. The first provides a comparison between model and recorded chemiluminescence images while the second technique allows point measurements to better quantify location specific cyclic behavior. The second technique uses broadband spectral imaging of flame emission via a fiber optic probe to reveal the species that contributed to light emission in past optically band-pass filtered imaging experiments. To complement new experimental data, a detailed chemical kinetics model that includes chemiluminescent species was employed in the computations to allow a direct comparison between the emitting species and infer a link to heat release. A brief history of previous research on the flame under investigation and a survey of investigations on chemiluminescence as a heat release indicator are presented in Section 2. Experimentation focuses on improving the quantitative nature of optical measurements and gaining insight on the use of combustion light emission as an indicator of heat release. Section 3 describes the experimental and modeling approach taken to investigate the heat release and chemiluminescent species distributions in a highly unstable flame. Results of spectroscopic imaging of the combustion light emission are compared to results from a CFD simulation of the flame, incorporating detailed chemical kinetics model in Section 4. An analysis is presented describing the simulated extraction of chemiluminescence data from the computational model. Finally, conclusions on the suitability of this approach for model validation for the subject flame are presented in Section 5.

2. Background

2.1 Review of CVRC Instability Modeling and Experimentation

The continuously variable resonance combustor (CVRC) was developed to study the mechanics of self-excited high frequency combustion instability in a practical rocket combustor. Gas phase propellants were used in a sub-scale single injector element configuration to remove inter-element interactions and liquid atomization physics, reducing the cost of computational modeling of the configuration.[8] The design allowed for characterization of the chamber acoustic field based on high frequency pressure measurements. Previous studies focused on high amplitude pressure oscillations in the combustor near the fundamental acoustic frequency, their harmonics, and their growth and decay.[8,9] Continuous variation of the oxidizer post length allowed for a resonance sweep from a quarter wave to a three-quarter wave resonant combustor.

Early modeling efforts showed reasonably good comparison with pressure fluctuations measured in the combustor. Self-excited instabilities could be predicted, but oscillation frequencies and limit cycle amplitudes differed from experimental results, a result that can be at least partly attributed to the adiabatic wall assumption in the model.[4,7,9] Early models relied on simple global chemical kinetic models to represent the complex methane oxidation reaction,[4] which resulted in differences in heat release magnitude and distribution between the model and experiment. CH* chemiluminescence, under the assumption that it is a heat release indicator, was used to characterize the fluctuating heat release distribution in the CVRC experiment. Due to line-of-sight integration of light emission signals and optical distortion caused by the glass combustor wall, comparisons between the experiment and model are limited in this regard.

2.2 Use of chemiluminescence as an optical diagnostic

Heat release rate in flames is a fundamental property involved in the evolution of unstable combustion behavior. To study heat release as it relates to interactions with acoustics requires a reliable indicator that is easily observable in experiments. Optical emissions from flames, including chemiluminescence, are commonly used as a combustion diagnostic because they are readily measurable with inexpensive detection equipment and occur naturally in the combustion process being observed. Chemiluminescence results from the relaxation of electronically excited species that are produced via chemical reactions in the combustion zone. In oxygen-hydrocarbon flames the species CH*, OH*, C_2*, and CO_2* are responsible for most of the light emission in

the visible and ultraviolet wavelengths.[10,11] By studying the light emission from these species, some insight can be gained about the energy release in the reaction zone of the flame.

The adequacy of chemiluminescence to indicate heat release from combustion reactions has been studied for decades. Much fundamental research has been performed on the topic using controlled burners in various configurations and using flames of varying equivalence ratio, strain rate, curvature, pressure, and reactant combinations. Early experiments made use of radical species emission as indication of heat release in both practical and laboratory combustors, but with no thorough understanding of the chemical reaction pathways from which the emitting species originated.[12,13] Later studies have investigated in detail the effects of variation in flame properties on chemiluminescence of several species.[14–32]

It is widely agreed that C_2* chemiluminescence is an inadequate indicator of heat release in the combustion reaction zone, as it is not spatially correlated with the heat release and is not associated with the major energy releasing reaction pathway for hydrocarbon flames. While C_2* chemiluminescence is more prevalent in fuel rich flames, it has been observed that the C_2* emission intensity increases monotonically, without any trend with respect to the equivalence ratio as it passes the stoichiometric value. Thus the C_2* emission does not trend with expected maximum heat release levels in the flame.[14,15] It is also suggested that C_2* is produced by a number of reactions in the overall kinetics model and thus may not compare uniquely to the heat release in a spatial or temporal sense.[17]

Extensive studies, both experimental and numerical, have shown that CO_2* emission could be considered a good indicator of integrated or total heat release and even local heat release for low turbulence flames. Samaniego et al.[18] showed that CO_2* chemiluminescence intensity varies monotonically but not uniquely with most flame properties, dependent upon which property is varied. Najm et al.[17] indicate that CO_2* emission may have a complex dependence on flame curvature and flow history, but has been shown to have maximum emission intensity near stoichiometric equivalence ratios.[14] Production of the CO_2* radical has been associated with the combination of CO and O near the end of the main carbon reaction in the methane oxidation reaction.[17–19]

Most commonly, chemiluminescence from the OH* and CH* species has been used as a combustion diagnostic, not only as a heat release indicator, but also to indicate other flame properties such as equivalence ratio and temperature.[20,21] Several studies involving premixed and diffusion flames at atmospheric pressure have indicated that OH* chemiluminescence is an important heat release marker because it coincides spatially with CH, a main reaction chain product.[14,16,20,22] Smith et al.[23] determined that the major production of OH* radicals is due to the reaction of CH molecules with O_2. Studies that observed OH* chemiluminescence in turbulent flames and flames with high strain rates reported poor agreement with heat release in that the emission varies strongly with turbulence levels and even disappears at high strain rates.[17,24–26] At elevated pressures, it has been suggested computationally that thermal excitation of OH molecules is the primary source for OH* radicals rather than chemical excitation that would be associated with the heat generating reaction path.[27]

Similar arguments either confirm[14,20] or deny[17,22,24,28] CH* chemiluminescence as an adequate heat release indicator. It has been shown that a quasi-steady state assumption for CH* production can be assumed reasonably, as CH* radicals are largely chemically excited[28,29] rather than thermally excited. In nearly all studies, the use of chemiluminescence as a heat release indicator is qualified on a case by case basis with variable results depending on strain rate, equivalence ratio, degree of turbulence, degree of premixing, and pressure of the flame. To remove the effects of flame property variation on the chemiluminescence, it has been shown that the ratios of certain species can be used to indicate equivalence ratio, independent of flame strain rate, but dependent on pressure and temperature.[14,30]

Recent studies have investigated laser induced fluorescence (LIF) techniques to excite intermediate reaction product species such as CH_2O and OH that are associated with the main chemical reaction chain in methane air flames.[25] Variability induced by spontaneous emission intensity is removed, however, LIF measurements are also challenging in high pressure flames due to collisional quenching of excited species and the high laser pulse energy required to produce a detectable fluorescence signal.

In summary, the heat release rate depends on equivalence ratio, mass flow rate, temperature, pressure, and local flame strain rate. In an unstable rocket combustor, each of these properties may vary widely, even on small length and time scales. Very little fundamental research has been performed on the ability of chemiluminescent species to indicate heat release in highly unsteady flames. Experimental chemiluminescence images of combustion behavior near the dump plane via two radical species, CH* and OH*, have been obtained for the unstable combustor configuration. Both of the species have been used as markers of heat release in various experiments,[28,31] but modeling of these radicals has been limited to relatively simple flames[20] and is rarely found in multi-dimensional simulations.[32] A major difficulty in their inclusion as a computed species

lies in the absence of their source species in the kinetics mechanisms that are typically used for the simulations. With a detailed kinetics model, like the GRI-1.2, this no longer is the case, and both CH* and OH* can be computed as quasi-steady species in a post-processing step with minimal computational cost. The assumption of quasi-steadiness can be expected to be better held for CH* than OH* because of its lower concentrations.[28]

3. Approach

3.1 Detailed Chemistry Models

Combustion instability is a manifestation of complex inter-dependencies of various processes occurring in a combustion chamber. To further understand the observations as well as to develop strategic knowledge, it is important to complement the experiments with modeling. High fidelity CFD models have shown promise in this regard.[3–7,9] Most of these models, however, utilize global reaction schemes, owing to the significant computational cost and challenges associated with detailed chemical kinetics models. Such models of methane combustion include between one and four reactions that attempt to reproduce the laminar flame speeds or species profiles.[33,34] In the case of premixed flames these aspects are important, but in the case of non-premixed flames, such as in the CVRC combustor, a more important characteristic is the induction period or ignition delay. This is the time taken by a mixture at a specified initial condition and composition to ignite. A comparison of the ignition delay predictions by various global mechanisms and the established detailed mechanisms is shown in Figure 1.

For conditions and compositions relevant to the CVRC operating conditions, the ignition delay predictions of the global mechanisms are one or more orders of magnitude shorter, and except in the case of single step mechanism, do not follow the trend of the detailed mechanism. Including detailed chemical kinetics is therefore beneficial to model the combustion instability, wherein accurate transients are important. In addition to improved reliability of the chemical kinetics model, inclusion of the detailed chemistry enables computation of radicals CH* and OH* that are observed through chemiluminescence imaging, thus allowing a direct comparison with the experiments. This merging of experimental and computational investigation is expected to shed light on the underlying physics of the coupling between combustion and fluid dynamics.

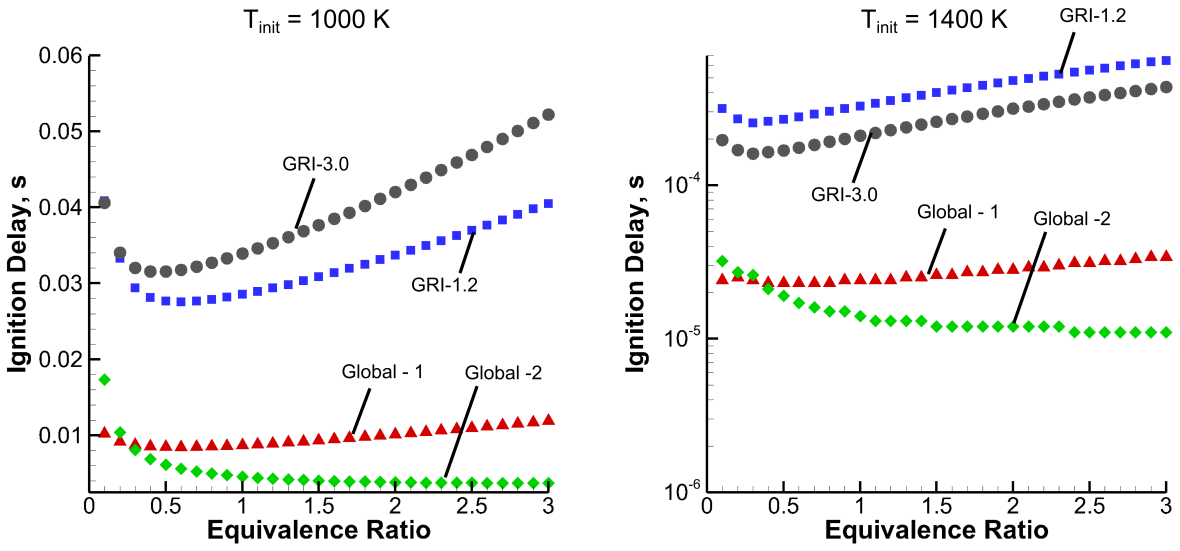

Figure 1: Comparison of ignition delay predictions for various mechanisms for compositions and conditions relevant to CVRC.

In the current study, we employ the reaction mechanism for CH* and OH* production and quenching presented by Hossain and Nakamura,[36] assuming quasi-steady state behavior of the two radicals and neglecting transport. Intensity of the chemiluminescence is obtained from the concentration of the radicals using the reported Einstein coefficient $A = 1.85 \times 10^6\, s^{-1}$. Volume integral corresponding to the viewing area of the optical probe is calculated and its phase average is plotted along with the pressure at the same location

to obtain a direct comparison with the experiments.

3.2 Experimental Configuration

As described previously, the CVRC test article has been used extensively to produce data sets for comparison to high fidelity CFD models.[4–8] The CVRC was designed to investigate the stability characteristics of an oxidizer centered shear-coaxial type injector element, common to oxidizer rich staged combustion engines, in a self excited unstable combustion environment. The oxidizer post length can be varied continuously during a test by changing the axial position of an orifice plate within the post. It has been shown by varying the resonant lengths of the combustor that the oxidizer post length plays a critical role in the stability of the injector element. In model validation experiments, the combustor burns decomposed 90% concentrated hydrogen peroxide and gaseous methane at a total equivalence ratio of 0.8, total mass flow rate of 0.345 kg/s, and average chamber pressure of 1.4 MPa. Although CFD modeling of the CVRC is performed using an oxidizer post length of 14 cm, in experimentation the oxidizer post length can be varied from 19 cm to 8.9 cm or fixed at any length in between. For translating oxidizer post tests, the post length is assumed to be quasi-static for small time intervals for comparison to computational models in which the geometry is fixed. In all cases in this discussion the oxidizer post length is 14 cm, a length associated with high amplitude instability. Figure 2 shows the combustor configuration. Head end chamber sections are interchanged dependent upon the type of measurements being performed.

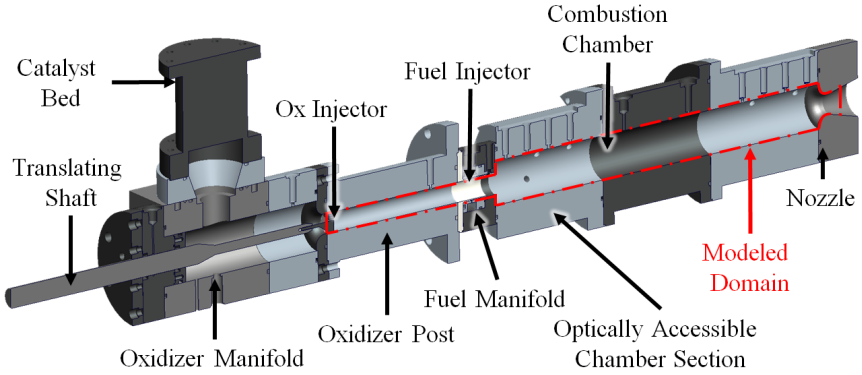

Figure 2: Cross section of the CVRC combustor. The head end chamber segment indicates location of fused quartz optically accessible chamber section and fiber optic ported chamber section. The computational domain is outlined by a red dashed line.

3.3 Chemiluminescence Imaging and Spectroscopy

Investigations of chemiluminescence in the CVRC combustor involve line of sight imaging of the combustor head end at 10 kHz frame rates through a fused quartz combustion chamber segment and optical band pass filters around wavelengths associated with OH* and CH* chemiluminescence near 309 nm and 431 nm respectively. The results offer two dimensional line-of-sight integrated spatial and temporal trends in relatively large wavelength bands of emitted light. Obscuration by the quartz glass combustor wall results in relatively low spatial resolution. Distortion from intensified imaging equipment required to collect emission signals in the UV-Visible spectrum also remove detail from collected images. The two dimensional images, when processed using Abel transform techniques, are able to provide qualitative comparisons of large scale general behavior between the experiment and computational model.

For improved spatial resolution of optical measurements and to increase the quantitative nature of the results, broadband spectral imaging of the CVRC combustion emission was performed using a fiber optic-coupled imaging spectrometer. The head end chamber section was replaced with one allowing integration of a 400 micron diameter fused silica fiber optic probe allowing collection of UV-Vis light emission. Several ports in the chamber allowed for line-of-sight light collection through the center-line of the combustion zone at various axial locations. As installed, the field of view of the fiber probe has an included angle of approximately 6.75 degrees extending 45 mm across the chamber diameter resulting in a probe volume of 717.2 mm^3. The

probe coupled light into a Horiba Scientific iHR550 imaging spectrometer with an entrance slit width of 0.2 mm. The spectrometer was configured with a 150 g/mm diffraction grating resulting in a spectral range of 265-470 nm for the detector used, capturing both OH* and CH* emission bands. Spectra were imaged at 10,000 samples/sec using a high speed UV intensifier and CMOS detector. Spectra and pressure data were collected simultaneously from an axial location located 23.8 mm downstream of the injector dump plane for direct comparison to computational model data. The hardware configuration is depicted in Figure 3.

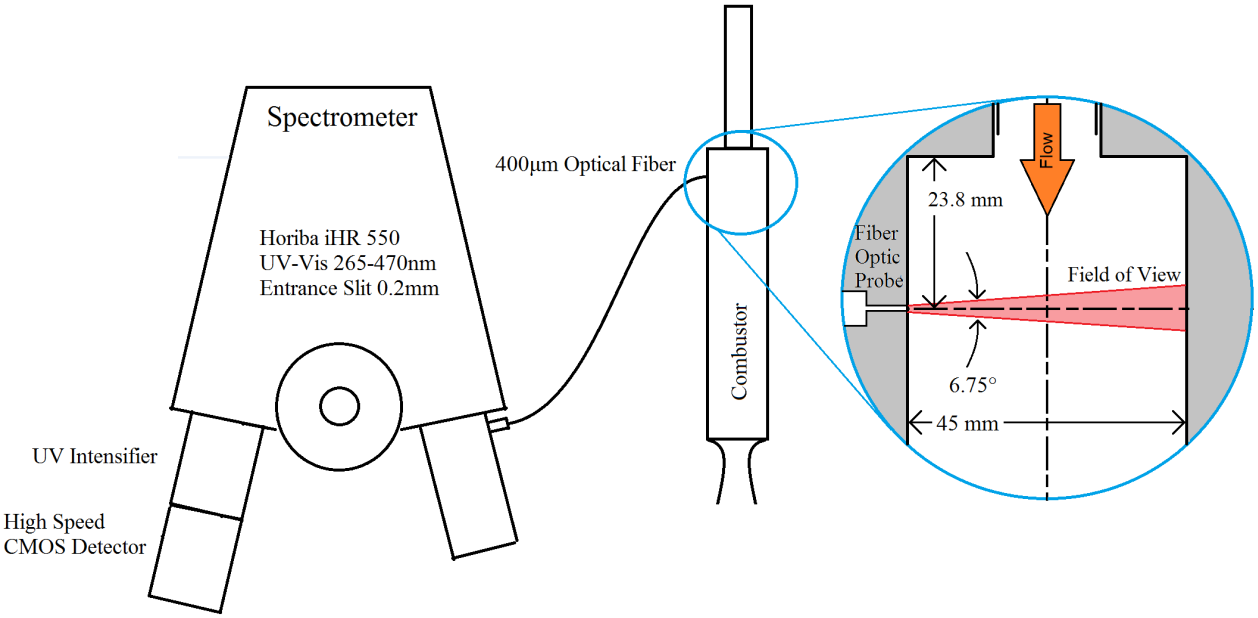

Figure 3: Configuration of spectroscopic imaging equipment.

3.4 Comparison of Model and Experimental Data

To extract model data that best represent experimental optical probe measurements, an understanding of the optical probe volume is required. The probe volume or field of view of the fiber optic probe used in this experiment is determined by the fiber diameter and the optic port geometry in the combustor chamber wall. The optic port in the chamber wall provides the limiting aperture in this case. The included angle of the probe volume, 6.75˚, was calculated using ray transfer matrix analysis of the most extreme ray captured by the probe. The analysis accounted for apertures at the fiber face and in the optic port in the chamber wall, refraction through the sapphire window at the bottom of the optic port, and relative distances of the components in the optic port. It was assumed that light transmitted to the fiber via reflections from hardware surfaces were negligible, no light was collected from within the optical port, refraction index gradients in the combustion gas were negligible, and that chemiluminescence for the wavelengths under investigation were not reabsorbed by the combustion gas, that is to say the gas is optically thin. The validity of this final assumption was investigated in depth as reabsorption of the emission signal may significantly skew the comparability of model and experimental data.

To represent this probe volume in the model data, the 2-D mesh was first revolved about its center axis, transforming it into a 3-D axisymmetric grid. Cell centers on this grid that fell within the probe volume were isolated, and the relative amount of light collected from each was determined using the ray transfer matrix analysis technique. Assuming diffuse emission of light from the center of each cell, a factor was calculated as the fraction of diffuse light emission collected by the optical fiber. A cross section of the probe volume in the computational domain is shown in Figure 4 where the points representing the cell centers are colored by the calculated fraction of the diffusely emitted light collected by the optic probe. It should be noted that a large fraction of the light is collected near the probe face, despite the smaller cross section of the probe volume, rapidly decreasing towards the end of the probe volume. It is therefore likely that the emission data collected will represent emission activity nearer to the combustor wall.

The second assumption, that the medium is optically thin, is critical to the direct comparison of experimental and model data, since re-absorption of light can significantly skew the line-of-sight integrated

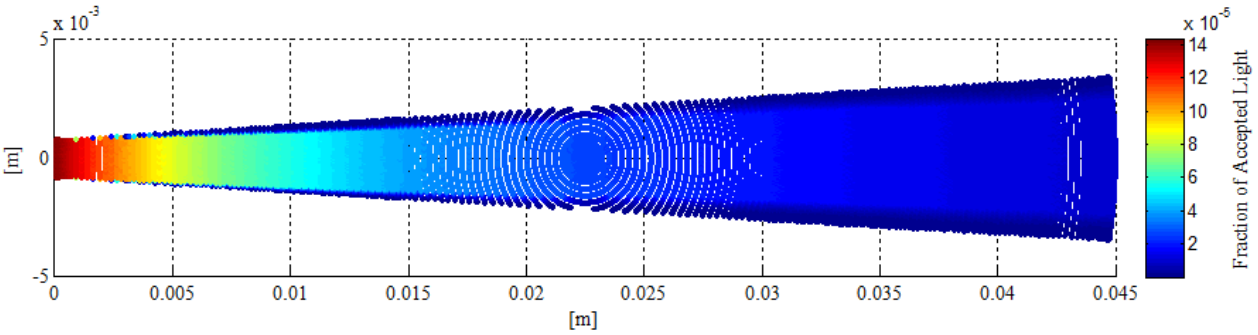

Figure 4: Cross section of optical probe volume colored by fraction of diffuse light collected from each cell based on ray transfer matrix analysis. Each data point represents the center of a cell in the revolved axisymmetric computational model. Variation in density of data points and circular groups of data points are caused by the revolution of the original 2-D axisymmetric mesh and cell density variation in the mesh.

optical measurements. In order to ascertain that no such skewness exists, optical depth analysis of the CH* and OH* data from computational model is performed.

The absorption fraction, α, is extracted from the Beer-Lambert law, and can be expressed as

$$\alpha = \frac{I}{I_0} = \exp(-K(n,\lambda)g(\lambda,T)z) = exp(-\sigma(\lambda,T)nz) \tag{1}$$

in terms of the ratio of transmitted to incident light, I/I_0, line strength, K, population number density, n, wavelength, λ, normalized line shape profile, g, temperature, T, and optical path length, z. A second form of the Beer-Lambert law is expressed using optical path length, macroscopic cross-section, σ, and number density directly.[37] Absorption and emissivity were first parametrically investigated for their dependence on number density, collisional line width, Doppler line width and optical path length.

Absorption or emission line strength is a function of number density and wavelength, while the line shape profile is a function of wavelength and temperature. The number density and optical path length were found to be the most significant parameters affecting the absorption fraction or emissivity. Since line strength is directly proportional to number density, from Equation 1 it is clear that the natural logarithm of the absorption fraction is directly proportional to both the number density and the optical path length.

The absorption properties of ground state OH and CH molecules are shown in Figure 5 where optical transmissivity is calculated as a function of number density for varying optical path lengths. This study was performed for the emission wavelengths of the OH* and CH* radicals. Transmissivity is the complement of the absorption fraction and reflects how well an electromagnetic wave at a particular frequency is able to propagate through an optical medium. It is clear that for a particular optical path length there is a threshold limit on number density of optical absorbers, above which complete optical absorption occurs.

The number densities of the absorbing species at the particular spectral wavelengths of interest within the probe volume can be predicted from the detailed chemical kinetics model as described previously. Figure 6 shows the number density averaged over the probe volume for a single pressure wave period of the emitting and ground state species of interest. In the case of CH, Figure 6a, the ground state population is sufficiently small to allow nearly complete transmission of CH* emission. This is not the case for the OH molecule, Figure 6b, where ground state populations are near or beyond the threshold value for significant absorption.

The maximum optical path length within the probe volume is the diameter of the chamber, which is approximately 0.045 m. Figure 6b shows that for nearly the entire pressure wave period, the OH* emission is completely absorbed over the longest optical path length. It should be noted that Figure 6represents the volume averaged number densities of the various species of interest, and localized variations in number density could be significant. The locally high OH number density greatly increases the optical thickness and as such the OH* emissions are likely completely absorbed suggesting that the collected emissions are produced near the surface of the combustor wall, near the optic probe face. Chemiluminescent OH*, therefore, may not be a good marker of the main reaction zone.In the case of CH* emission, Figure 6a shows that the number density of the corresponding ground state absorbers is low throughout the pressure period so that the products of combustion can be considered to be optically thin.

It is known that in high pressure flames, CO_2* chemiluminescence can be significant in a broadband spectrum encompassing the OH* and CH* emission wavelength bands. Figure 6 shows a relatively high

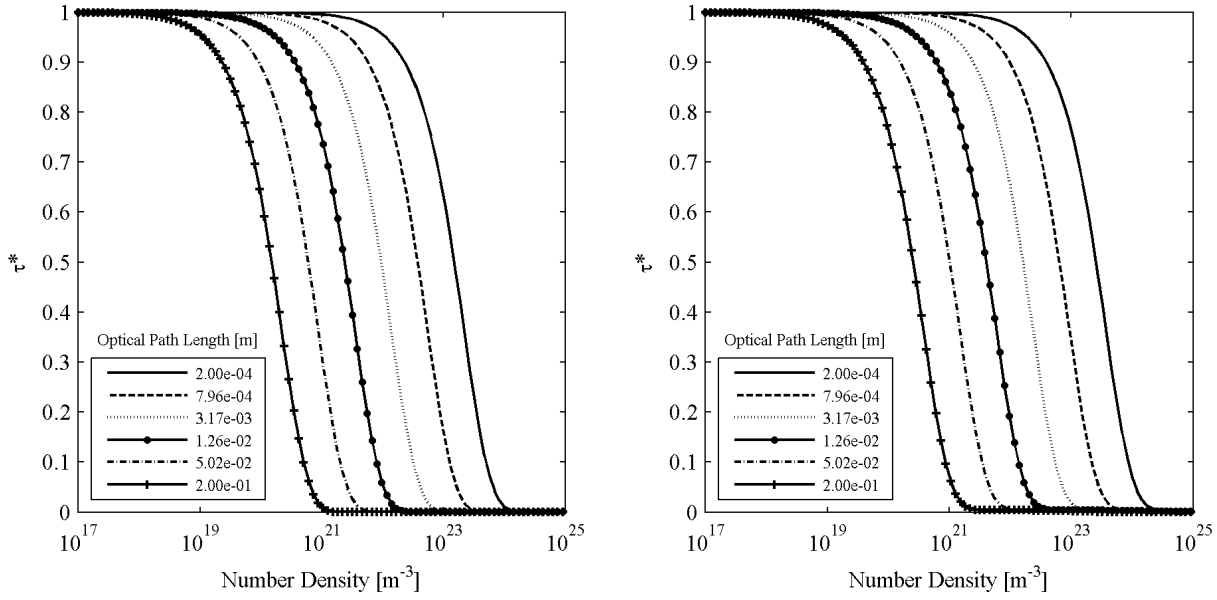

(a) CH (b) OH

Figure 5: (a) CH and (b) OH transmissivity as a function of number density for varying optical path lengths.

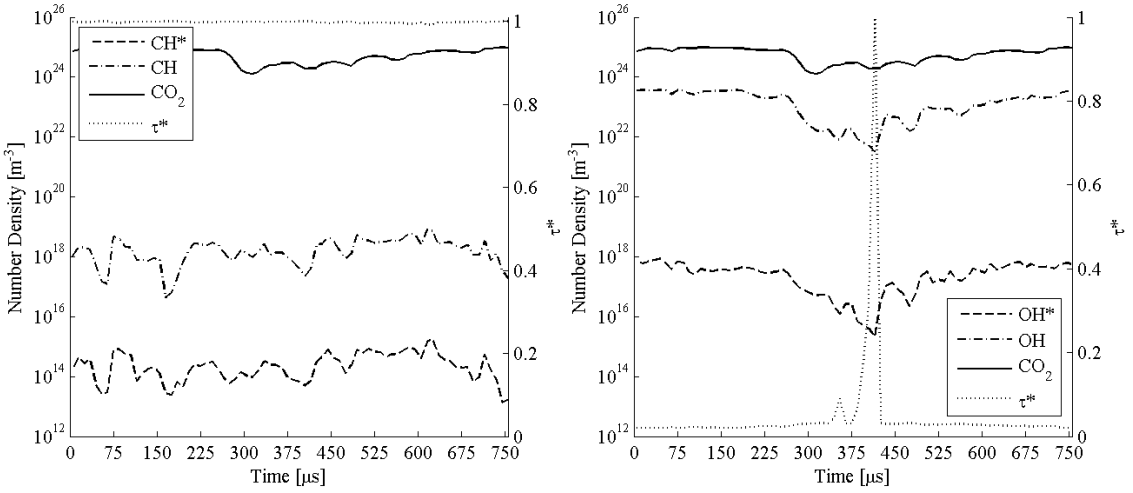

(a) CH (b) OH

Figure 6: Number density of emitting and absorbing species in the wavelength range of interest. Transmissivity of the medium to both (a) CH* and (b) OH* chemiluminescence are shown.

number density of CO_2 in the probe volume which is a potential absorber of OH* and CH* emissions. It was expected that since CO_2 emits within the spectral range of emissions from OH* and CH* that it would most likely contribute to the optical absorption within the same spectral range.

Using the semi-empirical macroscopic absorption cross-section relations developed by Oehlschaerger et al.[37] for the UV spectral range of hot CO_2, and extrapolating the data to fit the spectral range of interest, it was found that the macroscopic absorption cross-sections at the approximate gas temperature within the probe volume are extremely low. The order of magnitude of the cross-sections are low enough to offset the relatively high number density such that for the spectral range of wavelengths of interest CO_2 has an insignificant role in optical absorption of OH* and CH* chemiluminescence.

4. Results

4.1 General Behavior

A typical test of the CVRC begins with a period of oxidizer only flow to allow the hydrogen peroxide catalyst bed to reach operating temperature. Fuel flow is initiated and ignition is achieved by injection of a 12 mL JP-8 slug at 10 seconds. Translation of the oxidizer post choke plate begins at 11 seconds, reducing the oxidizer post length from 19 cm to 8.9 cm over 2 seconds during bi-propellant operation prior to shutdown. Pressure data recorded from the combustor head end is shown in Figure 7. The transition to unstable operation occurs at 12 seconds when the oxidizer post length is approximately 14.5 cm. The spectrogram of head end pressure in Figure 7 shows the transition to unstable operation and the corresponding oxidizer post length. Pressure oscillation amplitude is approximately 1 MPa with a fundamental frequency of 1312 Hz. The pressure oscillation is characterized by a steep-fronted pressure rise followed by a more gradual expansion as shown in Figure 8 with several smaller peaks caused by reflected waves and higher modal frequencies. Pressure measurements at several axial locations in the combustor and oxidizer post indicate traveling pressure waves, rather than standing waves, are present in the combustor at high oscillation amplitudes. This behavior is also observed in computational models.[3–7,9]

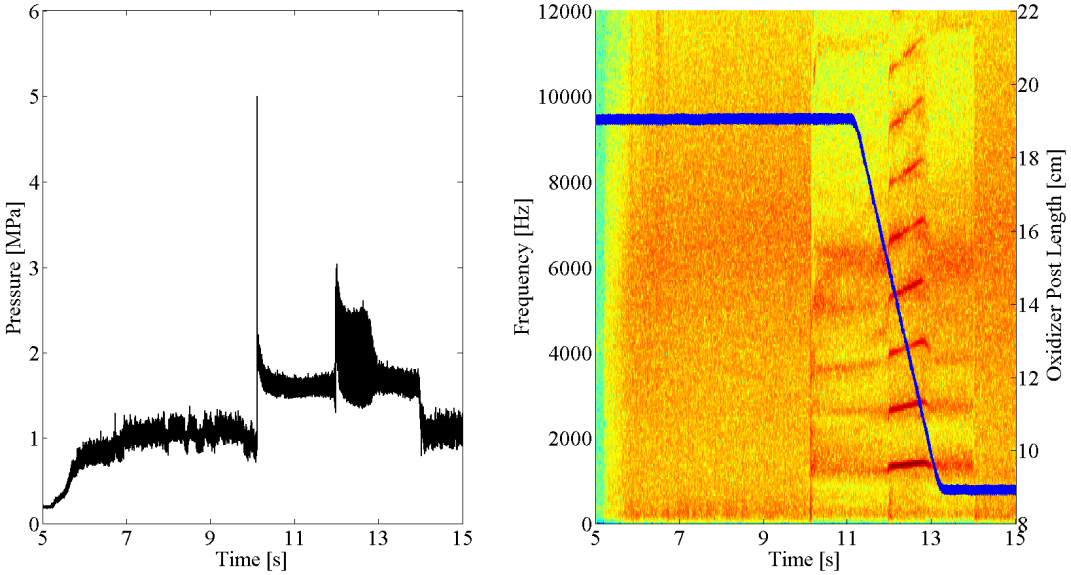

Figure 7: Typical head end chamber pressure trace (left) and spectrogram of head end pressure (right) comparing intensity of frequency content in pressure over time.

4.2 Chemiluminescence Imaging

The computational model in this study has the capability of predicting heat release with high spatial and temporal resolution, but there is no experimental measurement available to validate heat release predictions from the model. The reaction steps that were added to the chemical kinetics model to simulate CH* and OH* production enable an additional link for more direct comparison of experimental and model data. By linking the experimental and model data using the light emission and pressure signals, inferences can be drawn regarding the relative spatial and temporal heat release response based on that predicted by the model. Although any comparisons between the concentrations of emitters are qualitative, a temporal signal can be quite precise, therefore providing some level of confidence in the model.

The phase averaged pressure cycle at the head end of the combustor is shown in Figure 9, and the corresponding visual comparison is shown in Figure 10. The experimental images represent emission from the CH* radical. The images are inverse Abel transformed to account for line of sight measurements and phase averaged to diminish cycle to cycle variations. Simulation images are from axisymmetric computations

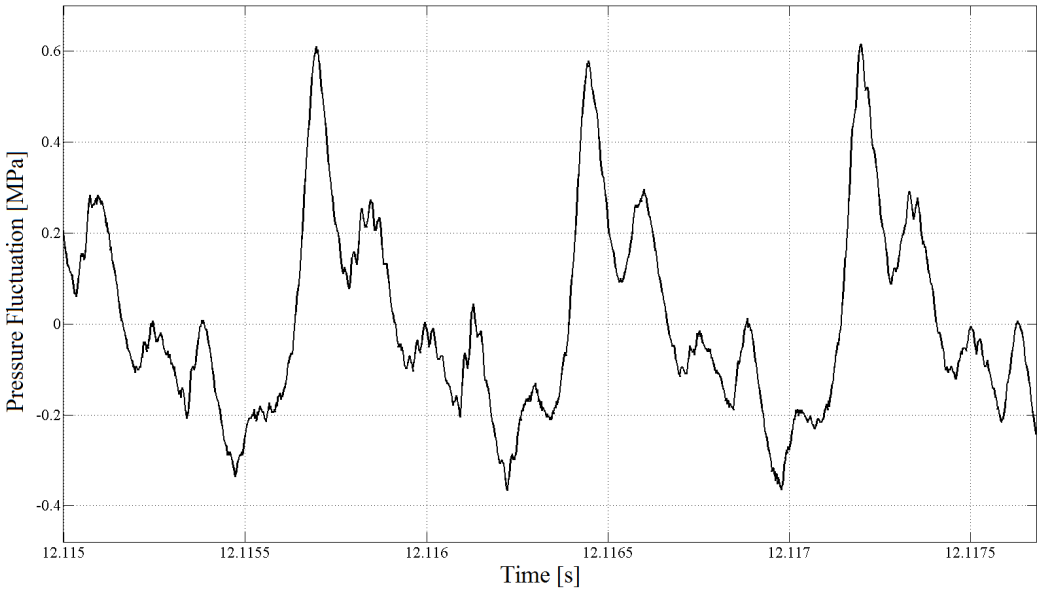

Figure 8: Typical pressure wave shape recorded in combustor head end.

and are similarly phase averaged. At the start of the cycle, during pressure rise, high intensity emission is seen near the wall of the combustor in both computational and experimental images. At or near the peak pressure, occuring at cycle point 3, the high intensity region displays a shift away from the wall. Pressure in the head end decreases from cycle points 7 to 15, while the luminosity of the CH* radicals indicates reduced number density. Towards the end of the cycle, points 18 to 20 show increasing intensity, marking the beginning of the next cycle. The same structural sequence can be seen in the computed CH* radical. The results suggest that the sequence of events starts with a partially mixed fuel-oxidizer jet hitting the combustor wall and rolling up to form two vortices. The upstream vortex interacts with the corner recirculation zone near the back step of the combustor. The corner recirculation zone contains hot products and, being on the periphery of the fuel-oxidizer mixture in the shear layer, forms a high concentration CH* region.

4.3 Spectroscopy of Chemiluminescent Emission

The average emission spectrum collected by the fiber optic probe during unstable operation of the CVRC is shown in Figure 11. The average spectrum indicates a strong emission from the $A^2\Sigma \Rightarrow X^2\Pi$ transition of OH* near 309 nm. Emission from the $A^2\Delta \Rightarrow X^2\Pi$ transition of CH* near 431 nm is significantly lower in average intensity, and light emission in this wavelength range is dominated by broadband CO_2* emission as expected from a high pressure lean hydrocarbon flame.[18] Two strong peaks at 328 nm and 338 nm are emission from atomic silver[38] that is eroded from the hydrogen peroxide catalyst bed. The spectrum is corrected for variation in the quantum efficiency of the imaging hardware over the wavelength range of interest.

To relate the unsteady heat release field to the strongly resonant flow, it is most useful to consider pressure phase locked average signals of light emission, thus averaging cycle-to-cycle variability. Phase averaging was performed over 25 pressure oscillation periods at the first longitudinal acoustic mode frequency of 1312 Hz. A cubic spline interpolation was performed to generate 50 data points per oscillation period and averaging was performed at each of these points. Although continuously translating, the average oxidizer post length during this interval is 14 cm, a thoroughly studied unstable configuration for the CVRC.[4,7–9]

To compare the relative intensities of the OH* and CH* emission signals, the CO_2* background emission was assumed to be self similar and was approximated by a fifth order polynomial as shown by Lauer[24] and subtracted from the spectra. It is evident in these spectra that the CH* emission signal is only slightly more intense than the noise level, but is still detectable despite the high pressure conditions of the flame. The phase averaged and normalized OH* and CH* emission signals are plotted against the phase averaged pressure signal in Figure 12. Comparison of the light emission and pressure signal shows that the peak OH* emission lags the peak pressure by about 40 degrees while the peak CH* emission leads the peak pressure by about 50 degrees on average. Thus, the total phase difference between peak OH* and CH* chemiluminescence

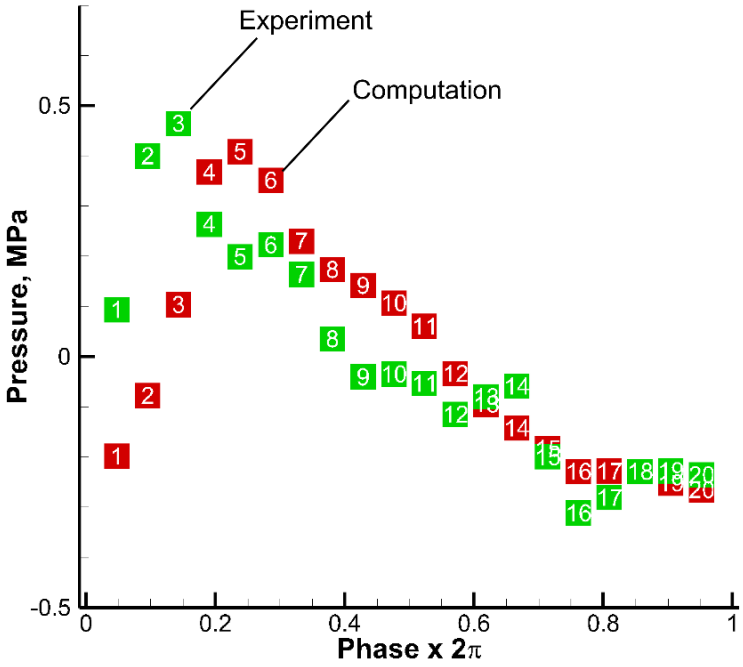

Figure 9: Phase averaged pressure cycle measured in the experiment (green) and predicted by computation (red).

is about 90 degrees. Although the line-of-sight nature of the measurement obscures the spatial detail of the flow field, the difference in phase of maximum OH* and CH* chemiluminescence suggests a distinct difference in the spatio-temporal evolution of the two species.

Data for OH* and CH* photon emission was collected from the computational domain using the probe volume geometry discussed previously. Pressure and heat release data were also collected and averaged over the probe volume to enable a more direct comparison to the emission signals. Figure 13 shows the pressure fluctuation, OH* and CH* emission intensities, and heat release rate averaged over 25 pressure cycles based on the computational model described previously.

Phase averaged pressure signals shown in Figure 14a during limit cycle operation show excellent agreement between the experiment and model data. Average amplitudes are well predicted for the duration of the pressure cycle. Figure 14b shows the comparison of phase averaged and normalized OH* emission intensity. This comparison reveals that although the general trend in OH* emission intensity is consistent between the model and the experiment, the maximum emission intensity predicted by the model is shifted in phase compared the signal measured in the experiment. This effect could either be due to the phase averaging or due to the assumption of quasi-steady state of this radical. Accurate phase averaging requires the cycle to be a smooth sinusoid, allowing for accurate determination of the phase. The steep fronted pressure cycle does not fit this requirement and can lead to errors in averaging. The assumption of quasi-steady state OH* radical is more expensive to deal with since it will require modeling production, destruction and transport of the additional species. Figure 14c shows the comparison of phase averaged CH* emission intensity. Phase angles of peak values of CH* emission as predicted in the computational model agree well with the experimental measurements. A secondary maximum occurs in the measured CH* signal at a phase angle of 200 degrees that is not predicted by the model and is not evident in the experimental or model data for the OH* emission. Although the general trend in CH* intensity is captured by the model, there are small features in the measured signal that are different from the model predictions. It should also be recognized here that the CH* signal may have some uncertainties due to the CO_2* extraction process and hence the overall trend seen should outweigh the details in the present comparison. The model does suggest a local maximum near 300 degrees that is not seen in the experimental data. Figure 14d compares chemiluminescent emission signals measured from the experiment to the heat release fluctuation predicted by the model on the basis of pressure

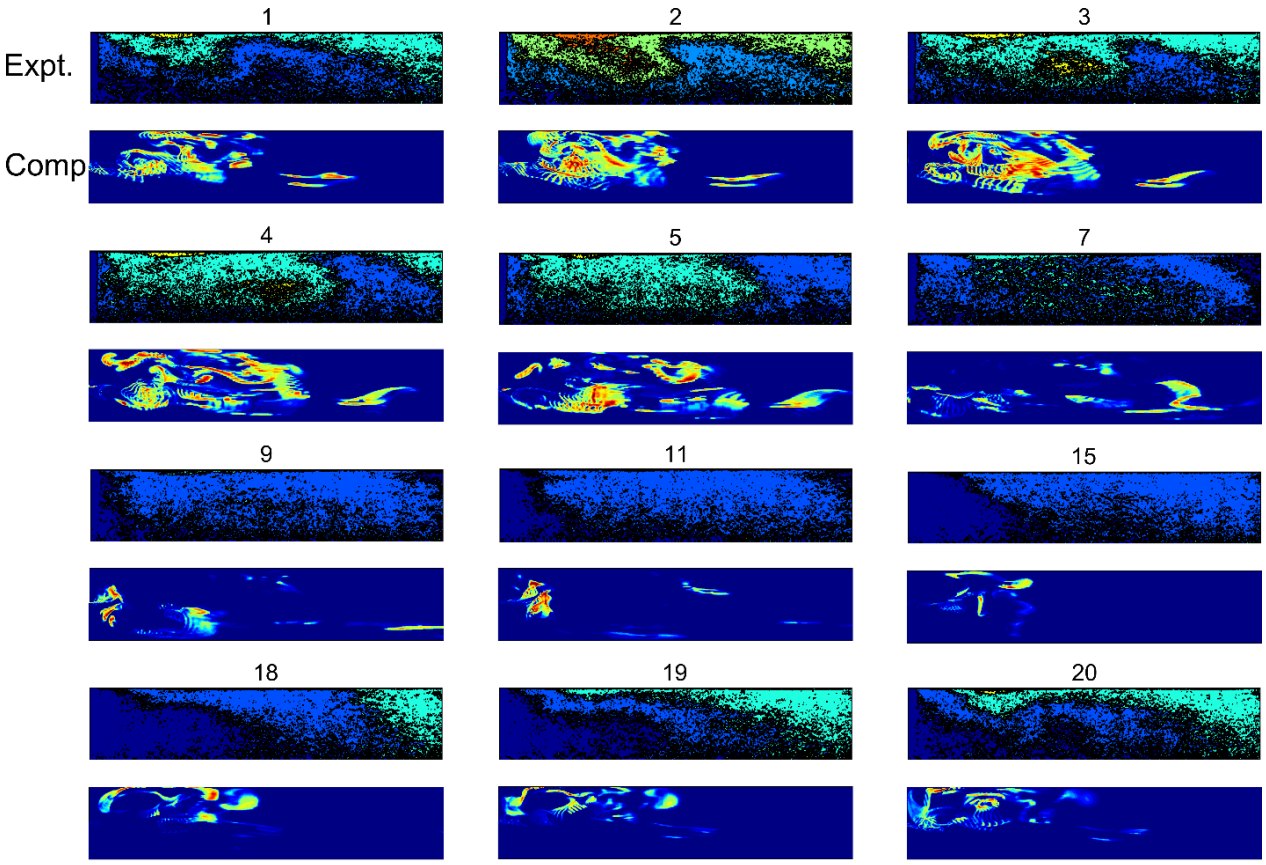

Figure 10: Inverse able transformed comparison between CH* chemiluminescence measured in the experiment (top) and predicted by computation (bottom).

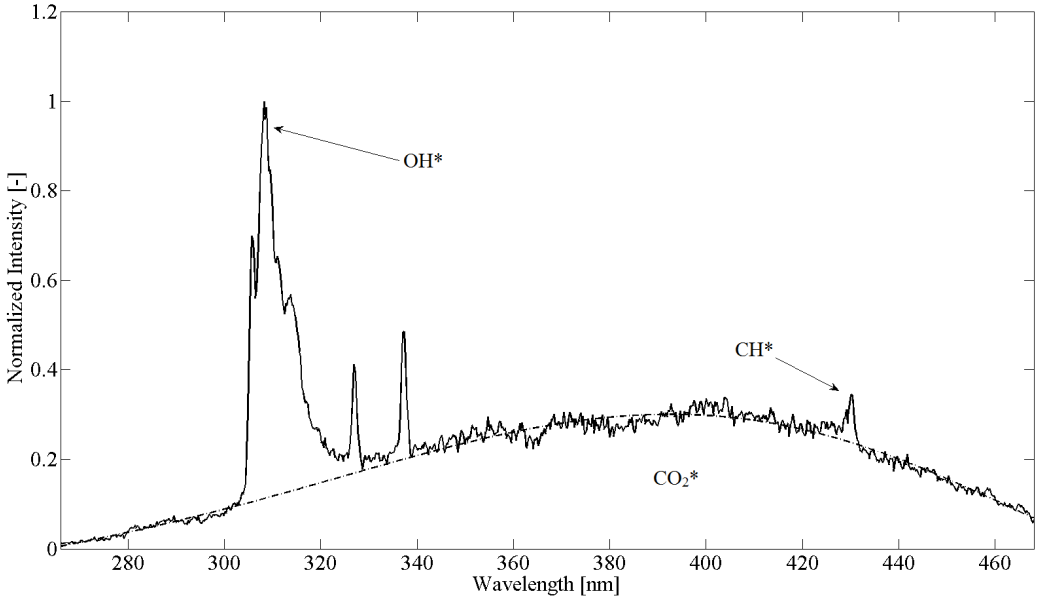

Figure 11: Average emission spectrum measured during unstable combustion indicating OH*, CH*, and CO_2* emission. Two strong lines at 328nm and 338nm are emission from atomic silver eroded from the hydrogen peroxide catalyst bed.[38]

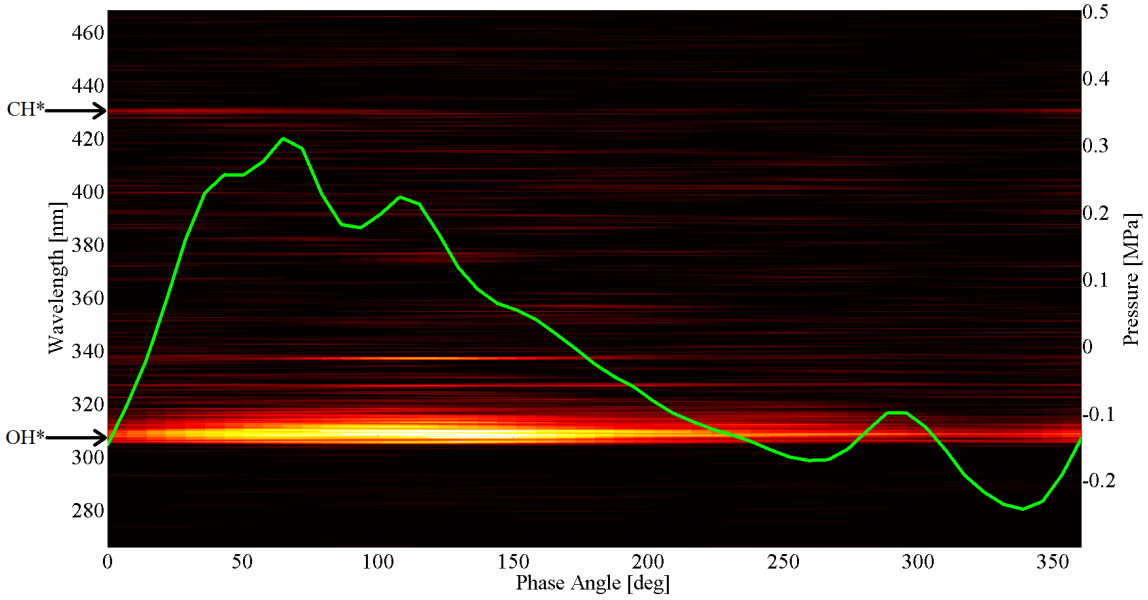

Figure 12: Phase averaged pressure (green) and emission spectrum for 25 phase averaged pressure oscillation periods measured at an axial location 23.8 mm downstream of the injector dump plane.

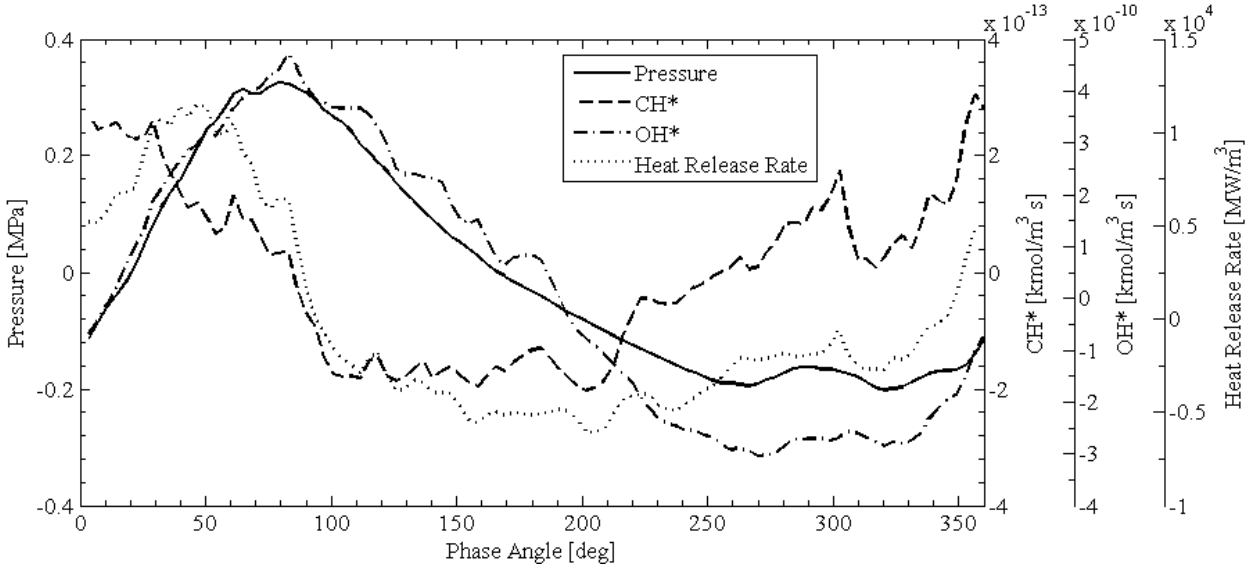

Figure 13: Phase averaged pressure heat release and radical species production rates measured from the computational model. OH* and CH* rates are determined by integrating throughout the probe volume with geometric weighting applied as discussed previously..

based phase averaging.

The model is able to predict the phase averaged pressure curve with trend-wise accuracy and, on this basis, the model heat release fluctuation and experimental emission measurements are compared directly, with the pressure curve providing the reference between the model and the experiment. Under the assumption that the model can accurately predict the timing of heat release with respect to the phase of the pressure signal, this result suggests that in line of sight integrated measurements neither OH* or CH* measurements are sufficient as indicators of heat release. The emission signals from both species are significantly out of phase with the predicted heat release in the probe volume. The peak CH* emission from the experiment leads the predicted peak heat release by approximately 30 degrees in terms of pressure phase angle while the

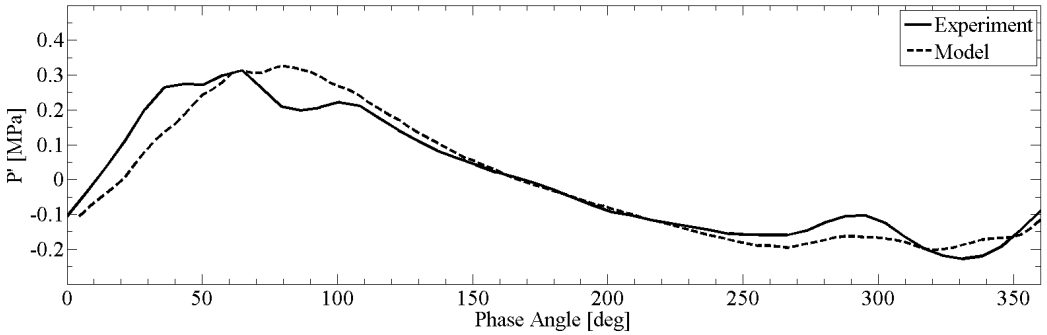

(a) Pressure

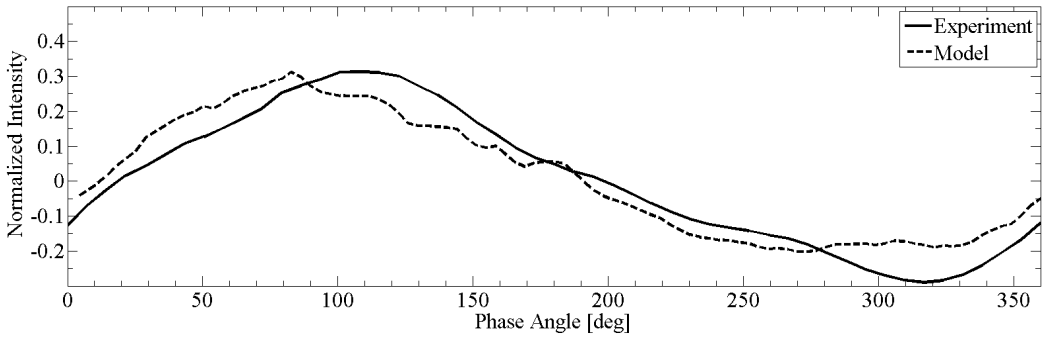

(b) OH*

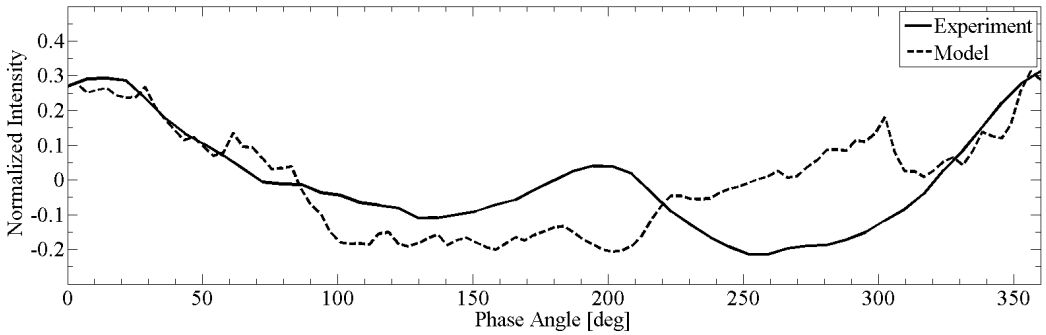

(c) CH*

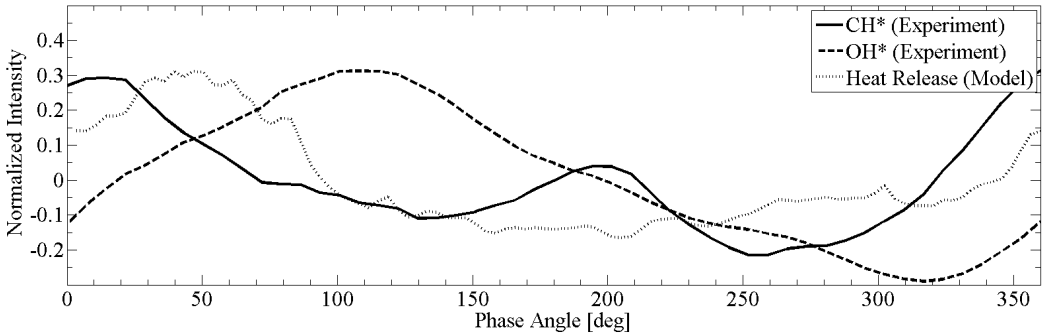

(d) CH*

Figure 14: Comparison of computational model and experimental data phase averaged by the oscillating pressure signal. a.) Pressure b.) OH* emission c.) CH* emission d.) Experimental OH* and CH* emission and model heat release.

peak OH* emission from the experiment follows predicted peak heat release by approximately 60 degrees. Considering that the model has captured the relative timing of chemiluminescent emissions from OH* and CH*, and neither of these signals appear to be able to directly indicate heat release suggests that neither signal can be quantified in other ways to determine the heat release location and magnitude directly, however, considering the turbulent nature of the reaction zone and line-of-sight integrated optical measurements, the combined experimental-computational approach towards chemiluminescent emission measurements described here does have the potential to provide an estimate of spatio-temporal trends in heat release fluctuations, and given the difficulties associated with both computations and measurements, simultaneous advancement is necessary to obtain quantifiable comparisons.

5. Conclusions

Measurements of the unsteady heat release field in a rocket combustor are key to understanding the mechanisms of combustion instability, validating high-fidelity simulations, and developing reduced-order models for combustion response. Although direct measurements are not presently possible, efforts to determine the best approximate method for a given application are needed. High-frequency measurements of the flame emission is a common means to acquire an approximate map of the time-dependent combustion field.

The most common species monitored for heat release are OH* and CH*, and previous studies have shown that their chemiluminescence intensities are functions of pressure, strain rate, equivalence ratio and turbulence level. Reacting flows in rocket combustors are highly intermittent, three-dimensional and turbulent with extreme rates of energy release. Local pressure can change by 50% in a fraction of a millisecond. Since the flame properties change so profoundly in space and time in a rocket combustor, it is difficult to decouple the emission from all other variables. Since line-of-sight integrated measurements of OH* and CH* obviously cannot provide a resolved mapping of heat release in this complex flow field, an appropriate simulation is needed for interpretation.

To allow a more direct means for comparing simulation and measurement, a predictive capability for CH* and OH* production was implemented into a detached eddy simulation of the experiment. The flame emission spectra between 265 and 470 nm were measured at 10,000 s^{-1} using a fiber optic probe. A model of emission in the probe volume was developed and applied to both the experiment and simulation. The emission model was also used to show that CH* is optically thin, and that significant self-absorption of OH* occurs.

The detailed chemistry model was able to predict the strong OH* emission and to some extent the weaker CH* emission intensity as observed in the experiment. Both experimental data and the detailed chemistry kinetics model indicate a phase difference in the line-of-sight integrated chemiluminescence measurements of OH* and CH* radical species at the location being investigated. Experimental phase averaged spectra indicate that the phase angle of peak CH* chemiluminescence is about 50 degrees ahead of the pressure peak, while the computational model predicts a phase lead of about 60 degrees. The phase angle of peak OH* chemiluminescence lags peak pressure by about 40 degrees as measured in the experiment, while in the computational model peak OH* chemiluminescence lags peak pressure by only about 7 degrees. Calculation of the radicals OH* and CH* from computations is based on the assumption of a quasi-steady state of the radical. While this is expected to be accurate for CH*, it may not be perfect in the case of OH* due to relatively higher concentrations and longer life of the OH* radical. A better way to compare OH* needs to consider it to be a transported species as a part of the kinetics mechanism. This modified approach is proposed for future computations.

Although literature suggests that the heat release cannot be compared directly to chemiluminescence in the experiment under all conditions, CFD model data reveal the spatial distribution of heat release in the combustor. The model suggests a strong spatial correlation between the heat release and the intensity of OH* and CH*. Considering only the volume observable by the fiber optic probe in the experiment, predicted heat release tends to follow CH* emission more closely than OH* emission, however on a phase averaged basis, both CH* and OH* emission exhibit a phase shift compared to predicted heat release. Under the assumption that the model can accurately predict the timing of heat release with respect to the phase of the pressure signal, this result suggests that neither line-of-sight measurement accurately indicates heat release. The CFD model shows a more complex set of interactions. The flame front and heat release zone is intricate with significant axial and radial variations. These effects cannot be observed in simple line-of-sight measurements commonly employed for observing high pressure turbulent flames. Motion of circulating flow through the probe volume may skew the observed phase relationship between heat release, pressure, and chemiluminescence intensity changes.

The average spectrum indicates that optically band-pass filtered images of high pressure turbulent combustion may contain substantial emission from species that are not necessarily of interest. In the case of lean, high pressure, turbulent, non-premixed flames such as that of the CVRC, CO_2* chemiluminescence is dominant in the CH* emission band and also has a significant contribution in the OH* emission band. Low CH* emission intensity in the CVRC flame makes detection difficult, and measurements may not have the fidelity required for resolution of spatial and temporal distributions. Therefore, one must use caution in analyzing CH* or OH* chemiluminescence images under the assumption that they represent energy release as they are affected by emission from other species.

The methods described here enable non-intrusive measurement of the combustion process that can be compared directly to simulation data. Fiber optic probes offer a robust and compact installation and allow for pressure measurement at coincident locations in small combustors. Refinement of the technique used here is recommended for future applications. Detectors with increased sensitivity would allow measurements at increased repetition rates and signal levels. A thorough understanding of optical probe volume geometry and opacity of the combustion gas to emission signals must be verified experimentally and is critical to improving confidence in comparisons to simulation data. Optical measurements should be located strategically and probe volumes optimized to provide the most insightful comparisons. Improvements in simulations such as modeling excited species transport and additional chemiluminescent species like CO_2*, as well as extending the domain to three dimensions, should be met with advancements in experimental measurement capabilities. Concurrent improvements in both simulations and experimental diagnostic techniques will improve understanding of unstable combustion dynamics in rocket combustors.

Acknowledgments

The authors would like to acknowledge support provided by AFOSR project FA9550-14-1-0029, with Dr. Mitat Birkan, Program Manager, graduate student William Z. Hallum for operation of the CVRC test stand to provide the presented test data, and Thomas Fiala of Technische Universität München and Mitsuaki Tanabe of Nihon University for their technical inputs to the project.

References

[1] Yang, V., and Anderson, W. E. Liquid Rocket Engine Combustion Instability, AIAA, Washington, DC, 1995.

[2] Sutton, G.P., Biblarz, O. Rocket Propulsion Elements. 7th Edition, John Wiley & Sons, New York, 2001.

[3] Smith, R., Ellis, M., Xia, G., Sankaran, V., Anderson, W. E., and Merkle, C. L. Computational Investigation of Acoustics and Instabilities in a Longitudinal-mode Rocket Combustor. *AIAA Journal*, Vol. 46, 11:2659-2673, November 2008.

[4] Harvazinski, M., Anderson, W., and Merkle, C. Analysis of Self-excited Combustion Instability Using Two and Three-Dimensional Simulations. *Journal of Propulsion and Power*, Vol. 29, 2:396-409.

[5] Garby, R., Selle, L., Poinsot, T. Large-Eddy Simulation of Combustion Instabilities in a Variable-length Combustor. *Comptes Rendus Mecanique*, 341:220-229, 2013.

[6] Srinivasan, S., Ranjan, R., and Menon, S. Flame Dynamics During Combustion Instability in a High-Pressure, Shear Coaxial Injector Combustor. *Flow Turbulence and Combustion*, Vol. 94, 1:237-262.

[7] Sardeshmukh, S. V., Anderson, W. E., Harvazinski, M. E., and Sankaran, V. Prediction of Combustion Instability with Detailed Chemical Kinetics. In *53rd AIAA Aerospace Sciences Meeting*, January 2015.

[8] Yu, Y., Sisco, J., Rosen, S., Madhav, A., and Anderson, W. Spontaneous Longitudinal Combustion Instability in a Continuously Variable Resonance Combustor. *Journal of Propulsion and Power*, 2012.

[9] Harvazinski, M., Huang, C., Sankaran, V., Feldman, T., Anderson, W., Merkle, C., and Talley, D. Instability Mechanism in a Pressure-Coupled Gas-gas Coaxial Rocket Injector. *AIAA Joint Propulsion Conference and Exhibit*, July 2013.

[10] Gaydon, A. G. The Spectroscopy of Flames. Chapman & Hall Ltd., London, 1957.

[11] Gaydon, A. G. and Wolfhard, H. G. Flames: Their Structure, Radiation, and Temperature. Chapman & Hall Ltd., London, 1960.

[12] Price, R. B., Hurle, I.R., and Sugden, T. M. Optical Studies of the Generation of Noise in Turbulent Flames. *Symposium on Combustion*, Vol. 12, 1:1093-1102, 1969.

[13] Hornstein, B., Budnik, C., and Courtney, W. Research Study of Light Emission Caused by Pressure FLuctuations in Rocket Engines. AFOSR Final Report No. 5520-F, March 1966.

[14] Hardalupas, Y. and Orain, M. Local Measurements of the Time-dependent Heat Release Rate and Equivalence Ratio Using Chemiluminescent Emission from a Flame. *Combustion and Flame*, Vol. 139, 188-207, 2004.

[15] Kathrotia, T., Riedel, U., Seipel, A., and Moshammer, K. Experimental and Numerical Study of Chemiluminscenct Species in Low-pressure Flames. *Applied Physics B.* 107:571-584, 2012.

[16] Kathrotia, T., Riedel, U., Warnatz, J. A Numerical Study on the Relation of OH*, CH*, and C_2* Chemiluminescence and Heat Release. In *Proceedings of the European Combustion Meeting*, 2009.

[17] Najm, H., Paul, P., Mueller, C., and Wyckoff, P. On the Adequacy of Certain Experimental Observables as Measurements of Flame Burning Rate. *Combustion and Flame*, 113:312-332, 1998.

[18] Samaniego, J., Egolfopoulos, F., and Bowman, C. CO_2* Chemiluminescence in Premixed Flames, *Combustion Science and Technology*, 109:183-203, 1995.

[19] Clyne, M. A. A. and Thrush, B. A. Mechanism of Chemiluminescent Combination Reactions Involving Oxygen Atoms. *Proceedings of the Royal Society of London. Series A, Mathematical and Physical Sciences.* Vol. 269, 1338:404-418, September 1962.

[20] Panoutsos, C., Hardalupas, Y., and Taylor, A. M. K. P. Numerical Evaluation of Equivalence Ratio Measurement Using OH* and CH* Chemiluminescence in Premixed and Non-premixed Methane-Air Flames. *Combustion and Flame*, 156:273-291, November 2008.

[21] Sandrowitz, J. and Cooke, G. N. Flame Emission Spectroscopy for Equivalence Ratio Monitoring. *Applied Spectroscopy*, Vol. 52, 5:658-662, 1998.

[22] Haber, C., Vandsburger, W., Saunders, W., and Khanna, V. An Experimentation of the Relationship Between Chemiluminescent Light Emissions and Heat-release Rate Under Non-adiabatic Conditions. *RTO AVT Symposium on Active Control Technology for Enhanced Performance Operational Capabilities of Military Aircraft, Land Vehicles, and Sea Vehicles*, MP-051, Braunschweig, Germany, 8-11 May, 2000.

[23] Smith, G. P., Luque, J., Park, C., Jeffries, J. B., and Crosley, D. R. Low Pressure Flame Determinations of Rate Constants for OH(A) and CH(A) Chemiluminescence. *Combustion and Flame*, 131:59-69, 2008.

[24] Lauer, M. and Sattelmayer, T. On the Adequacy of Chemiluminescence as a Measure for Heat Release in Turbulent Flames with Mixture Gradients. *Journal of Engineering for Gas Turbines and Power*, Vol. 132, 061502, June 2010.

[25] Ayoola, B., Balachandran, R., Frank, J., Mastorakos, E., and Kaminski, C. Spatially Resolved Heat Release Rate Measurements in Turbulent Premixed Flames. *Combustion and Flame*, 144:1-16, 2006.

[26] Farhat, S., Ng, W., and Zhang, Y. Spatially Resolved Heat Release Rate Measurements in Turbulent Premixed Flames. *Fuel*, 84:1760-1767, 2005.

[27] Fiala, T. and Sattelmayer, T. On the Use of OH Radiation as a Marker for the Heat Release Rate in High-pressure Hydrogen-oxygen Liquid Rocket Combustion, *49th AIAA/ASME/SAE/ASEE Joint Propulsion Conference and Exhibit*, 2013.

[28] Nori, V. N. and Seitzman, J. M. CH* Chemiluminescence Modeling for Combustion Diagnostics. *Proceedings of the Combustion Institute*, Vol. 32, 895-903, 2009.

[29] Elsamra, R. M., Vranckx, S., Carl, S. A. CH (A2δ) Formation in Hydrocarbon Combustion: The Temperature Dependence of the Rate Constant of the Reaction $C_2H+O_2 \rightarrow$ CH (A2δ) + CO_2. *The Journal of Physical Chemistry A*, Vol. 109, 45:10287-10293.

[30] Nori, V. N. and Seitzman, J. M. Evaluation of Chemiluminescence as a Combustion Diagnostic Under Varying Operating Conditions. *46th AIAA Aerospace Sciences Meeting and Exhibit*, 2008.

[31] Higgins, B., McQuay, M., Lacas, F., Rolon, J., Darabiha, N., and Candel, S. Symmetric Measurements of OH* Chemiluminescence for Fuel Lean High Pressure Premixed Laminar Flames. *Fuel*, 2001.

[32] Walsh, K., Long, M., Tanoff, M., and Smooke, M. Experimental and Computational Study of CH, CH*, and OH* in an Axisymmetric Laminar Diffusion Flame. *Symposium (international) on Combustion*. Vol. 27, 1:615-623.

[33] Westbrook, C. and Dryer, F. Simplified Reaction Mechanism for the Oxidation of Hydrocarbon Fuels in Flames. *Combustion Science and Technology*, Vol. 27, 31-43, 1981.

[34] Jones, W. and Lindstedt, R. Global Reaction Schemes for Hydrocarbon Combustion. *Combustion and Flame*, Vol. 73, 233-249, 1988.

[35] Frenklach, M., Wang, H., Goldenberg, M., Smith, G., Golden, D., Bowman, C., Hanson, R., Gardiner, W., and Lissianski, V. GRI-Mech-1.2, An Optimized Detailed Chemical Reaction Mechanism for Methane Combustion, Tech. rep., Gas Research Institute, 1995.

[36] Hossain, A. and Nakamura, Y. A Numerical Study on the Ability to Predict the Heat Release Rate Using CH* Chemiluminescence in Non-sooting Counterflow Diffusion Flames. *Combustion and Flame*, Vol. 161, 1:162-172, 2014.

[37] Oehlschaeger, M.A., Davidson, D.F., Jeffries, J.B., and Hanson R.K. Ultraviolet Absorption Cross-sections of Hot Carbon Dioxide. *Chemical Physical Letters*, 490-495, November 2004.

[38] Watanabe, H. and Kendall, K. Flame Spectrograms: I. Common Metals. *Applied Spectroscopy*, Vol. 9, 3:132-140, 1955.